Research Square

Preprints are preliminary reports that have not undergone peer review.
They should not be considered conclusive, used to inform clinical practice,
or referenced by the media as validated information.

Foxk2 regulates osteoblast differentiation and bone formation through Slc1a4-mediated enhancement of glutamine-dependent energy metabolism

Songlin Peng

pengsonglin@mail.sustech.edu.cn

Shenzhen People's Hospital(The Second Clinical Medical College, Jinan University; The First Affiliated Hospital, Southern University of Science and Technology)

Chungeng Liu

Guangdong Cardiovascular Institute, Guangdong Provincial People's Hospital, Guangdong Academy of Medical Sciences, Southern Medical University

Junfei Zhao

Guangdong Cardiovascular Institute, Guangdong Provincial People's Hospital, Guangdong Academy of Medical Sciences, Southern Medical University

Jian Liu

Guangdong Cardiovascular Institute, Guangdong Provincial People's Hospital, Guangdong Academy of Medical Sciences, Southern Medical University

Zhenmin Wang

Shenzhen People’s HospitalShenzhen Key Laboratory of Musculoskeletal Tissue Reconstruction and Function Restoration

Kangyan Zheng

Shenzhen People’s HospitalShenzhen Key Laboratory of Musculoskeletal Tissue Reconstruction and Function Restoration

Yongheng Xie

Shenzhen People's Hospital (The Second Clinical Medical College, Jinan University; The First Affiliated Hospital, Southern University of Science and Technology)

Jinchi Dai

Guangdong Cardiovascular Institute, Guangdong Provincial People's Hospital, Guangdong Academy of Medical Sciences, Southern Medical University

Houqing Long

Shenzhen People's Hospital(The Second Clinical Medical College, Jinan University; The First Affiliated Hospital, Southern University of Science and Technology) https://orcid.org/0000-0003-4480-7298

Article

Keywords:

Posted Date: March 3rd, 2026

DOI: https://doi.org/10.21203/rs.3.rs-8690219/v1

License: This work is licensed under a Creative Commons Attribution 4.0 International License.
Read Full License

Additional Declarations: There is **NO** Competing Interest.

Foxk2 regulates osteoblast differentiation and bone formation through Slc1a4-mediated enhancement of glutamine-dependent energy metabolism

Chungeng Liu[1,2,3,#], Junfei Zhao[1,#], Jian Liu[1,#], Zhenmin Wang[2,3], Kangyan Zheng[2,3], Yongheng Xie[2,3], Jinchi Dai[1], Houqing Long[2,3]*, Songlin Peng[2,3]*

[1] Department of Cardiovascular Surgery, Guangdong Cardiovascular Institute, Guangdong Provincial People's Hospital, Guangdong Academy of Medical Sciences, Southern Medical University, Guangzhou, China.

[2] Division of Spine, Department of Orthopedic Surgery, Shenzhen People's Hospital (The Second Clinical Medical College, Jinan University; The First Affiliated Hospital, Southern University of Science and Technology), Shenzhen, 518020, Guangdong, China

[3] Shenzhen Key Laboratory of Musculoskeletal Tissue Reconstruction and Function Restoration, Shenzhen, China

[#]Chungeng Liu, JunFei Zhao and Jian Liu contributed equally to this work.

*Corresponding authors:

Telephone number: +86-0755-25533018

Emails:

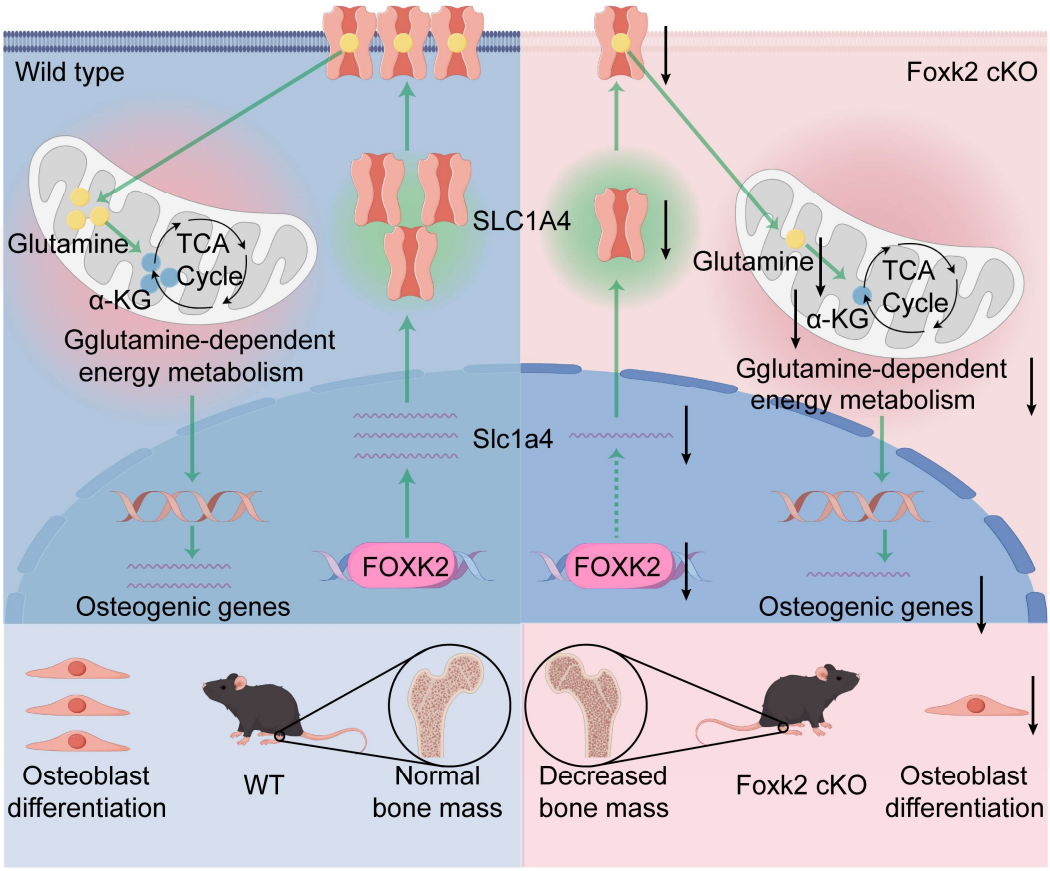
Songlin Peng: pengsonglin@mail.sustech.edu.cn

Houqing Long: houqinglong@163.com

Abstract

Foxk2 can regulate cell differentiation, proliferation, metabolism and tumor fate. However, the roles of Foxk2 in bone formation are unknown. Here, we found that global knockout of Foxk2 in mice resulted in decreased bone mass and bone formation. Deletion of Foxk2 in primary pre-osteoblasts suppressed osteoblast differentiation *in vitro* and conditional knockout of Foxk2 in pre-osteoblasts in mice showed attenuated bone mass and bone formation. Notably, overexpression of Foxk2 in pre-osteoblasts alleviated bone loss in mice caused by ovariectomy. Mechanistically, we identified Slc1a4 as a downstream target of Foxk2 through joint analysis the data of RNA-Seq and CUT&Tag. Knockout of Slc1a4 in pre-osteoblasts in mice resulted in decreased bone mass and bone formation. Overexpression of Slc1a4 in pre-osteoblasts alleviated bone loss and damaged bone formation caused by Foxk2 deletion. Furthermore, metabolomic analyses highlighted the role for Foxk2 in promoting glutamine-dependent energy metabolism mediated by Slc1a4, which is required for osteoblast differentiation. In summary, our study demonstrated that Foxk2 promotes osteoblast differentiation and bone formation through Slc1a4-mediated enhancement of glutamine-dependent energy metabolism, which is also a promising target for preventing osteoporosis.

Graphic abstract



Introduction

Osteoporosis, as a growing public and severe health problem, imposes a heavy economic burden on society and families. The characteristics of osteoporosis are loss of bone mass and degeneration of bone microarchitecture, leading to an increased risk of fractures[1]. Bone tissues are in a continuous dynamic remodeling process, which is regulated by the close interaction between osteoblasts (responsible for bone formation) and osteoclasts (responsible for bone resorption)[2]. The disruption of these balances, namely the activity of bone resorption exceeds bone formation, causes osteoporosis[2]. The current main treatment for osteoporosis focuses on inhibiting bone resorption by targeting osteoclasts, but these therapeutic drugs come with numerous side effects, including atypical femoral fractures and jawbone necrosis[3, 4]. Two classes of anabolic drugs, parathyroid hormone and parathyroid hormone-related protein, are now available to stimulate bone formation[4, 5]. However, anabolic drugs are expensive, require frequent injections, and have the potential to promote the development of osteosarcoma[4, 5]. Therefore, there remains a clinical need to explore the mechanism of bone formation in order to identify targets for treating osteoporosis.

Osteoblasts are the chief bone-making cells and produced throughout life from mesenchymal progenitors during bone remodeling and fracture healing[6]. The recognized signaling that stimulates osteoblast differentiation includes bone morphogenetic proteins, modulators of Wnt signaling, and parathyroid hormone (PTH) peptide application[7]. In recent years, metabolism has been recognized as playing a crucial role in regulating osteoblast differentiation and function. Glutamine is the most abundant non-essential amino acid in circulation and possesses various biological functions. The initial step of glutamine metabolism is the deamination of glutaminase to generate glutamate. In addition to direct contribution to protein synthesis, glutamine can supply α-ketoglutarate (α-KG) for the TCA cycle to participate in cellular energy production. Glutamine is an essential nutrient for osteoblast differentiation and bone formation[8, 9]. Glutamine metabolism plays a role in PTH and WNT3A induced bone formation[9]. However, the underlying mechanisms of mediating glutamine metabolism in osteoblast are not fully understood.

Foxk2 is the member of the fork head box (FOX) transcription factor superfamily, which involved in cell proliferation, autophagy, differentiation and metabolism[10-13]. Foxk2 has been mostly studied in the context of cancer biology, recognized as a regulator in ovarian cancer, breast cancer**,** and colorectal cancer[14-16]. Foxk2 can promote aerobic glycolysis and mediate mitochondrial metabolism by regulating related genes encoding related enzymes[13, 17]. Foxk2 promotes airway remodeling during chronic asthma by enhancing glycolysis in a SIRT2-dependent manner[18]. Foxk2 influences cancer cells response to chemotherapy by promoting de novo nucleotide synthesis[19]. Despite the important role of Foxk2 in metabolic regulation, it remains to be explored whether Foxk2 may regulate osteoblast metabolism during osteoblast differentiation, and how exactly this regulation contributes to bone formation.

Here, we revealed that Foxk2 is a critical regulator of osteoblast metabolism and bone formation. We demonstrated that deletion of Foxk2 suppressed osteoblast differentiation and bone formation and overexpression of Foxk2 in pre-osteoblasts could delay the progression of osteoporosis caused by ovariectomy. Through RNA-seq, CUT&Tag and bioinformatics analyses, we identified Slc1a4*,* which is a neutral amino acid transporter, as a direct target of Foxk2 in osteoblasts. Loss of Slc1a4 in pre-osteoblast impaired osteoblast differentiation and bone formation. Overexpression of Slc1a4 could rescued the weakened bone formation caused by knockout of Foxk2. Furthermore, metabolomic analyses indicated that the Foxk2/Slc1a4 axis promoted the glutamine metabolism required for osteoblast differentiation. Thus, our study demonstrated that Foxk2 promotes bone formation by regulating Slc1a4 mediated glutamine metabolism in osteoblasts.

Results

Foxk2 KO mice exhibit low bone mass

Deficiency of Foxk1 in mice is associated with low bone mass and decreased bone formation[20]. These findings lead us to examine whether Foxk2 also has a role in bone metabolism, especially in bone formation. To investigate the role of Foxk2 in bone formation, we generated *Foxk2-Knockout* mice (*Foxk2 KO*) (Supplementary Fig. 1a) and confirmed that Foxk2 was effectively deleted by using qPCR and western blot

(Supplementary Fig. 1b, 1c). *Foxk2 KO* mice were smaller and lighter than their wild type littermates at 8 weeks of age in both male and female mice (Supplementary Fig. 1d, 1e). The microCT analysis of femur metaphysis revealed that Foxk2 deletion caused bone mass reduction in both male and female mice (Fig. 1a). The bone volume (BV), bone volume/tissue volume ratio (BV/TV) and trabecular number (TB.N) were significantly reduced in *Foxk2 KO* mice compared to the control mice (Fig. 1b-1d), while the trabecular separation (Tb.Sp) increased (Fig. 1e). Biomechanical testing demonstrated that *Foxk2 KO* resulted in an overall deterioration in biomechanical properties characterized by markedly reduced maximum bending strength, and elastic modulus (Fig. 1f and 1g). H&E staining also showed that the trabecular bone area and number reduced in *Foxk2 KO* mice compared to control mice (Fig. 1h).

Next, we performed calcein double labeling to analyze dynamic bone formation in *Foxk2 KO* mice. The results showed that Foxk2 deletion weakened the bone formation activity, as indicated by decreased mineral apposition rate (MAR) and bone formation rate (BFR) (Fig. 1i-1k). Osteocalcin (OCN) IHC staining revealed reduced number of osteoblasts on trabecular bone surface in *Foxk2 KO* mice compared to WT mice (Fig. 1l and 1m), which is consistent with the reduced ossification and bone formation rate. Furthermore, western blot showed reduced osteogenic markers expression, including RUNX2, OSTERIX, ALP and OCN, in *Foxk2 KO* mice femoral tissue compared to control mice (Supplementary Fig. 1f). These findings suggest that Foxk2 may affect bone formation by regulating osteoblast differentiation *in vivo*. Interestingly, the results of tartrate resistant acid phosphatase (TRAP) staining demonstrated that loss of Foxk2 also resulted in reduction of osteoclast number (Fig. 1n and 1o), suggesting that Foxk2 also controls osteoclastogenesis *in vivo*.

Deletion of Foxk2 inhibits osteoblast differentiation

In order to determine the intrinsic role of Foxk2 in osteoblasts, primary murine calvarial osteoblasts (pre-osteoblasts) were isolated from *Foxk2 ko* and WT neonatal mice and were induced osteoblast differentiation. We found that Foxk2 expression significantly increased on the third day (day 3) of osteoblast differentiation and remained at a high level on day 7 (Supplementary Fig. 2a and 2b), which indicated that

Foxk2 plays a positive role in osteoblast differentiation. Deletion of Foxk2 decreased the osteogenic marker genes expression, including Runx2, Osterix, Col1a1 and Alp (Supplementary Fig. 2d-2g). These findings were further confirmed by the result of western blotting, showing that RUNX2, OSTERIX and ALP protein levels reduced in *Foxk2 KO* primary pre-osteoblasts compared to control cells (Supplementary Fig. 2h). Furthermore, deletion of Foxk2 attenuated ALP staining and Alizarin Red S (ARS)-stained mineralized nodules (Supplementary Fig. 2i). These finds demonstrated that Foxk2 positively regulates osteoblast differentiation.

Loss of Foxk2 in Pre-osteoblasts causes reduced bone mass

We next generated pre-osteoblast specific knockout of Foxk2 mice by mating the *Osterix-Cre* (*Osx-cre*) transgenic mice with *Foxk2*$^{fl/fl}$ mice (Supplementary Fig. 3a) to further investigate the influence of osteoblastic Foxk2 on bone formation *in vivo*. IHC staining revealed that the expression of FOXK2 significantly decreased in *Osx-cre;Foxk2*$^{fl/fl}$ mice femur (Supplementary Fig. 3b). IF staining images showed that the OSTERIX positive cells significantly decreased in *Osx-cre;Foxk2*$^{fl/fl}$ mice, with the reduction of Foxk2 (Supplementary Fig. 3c). qPCR further confirmed the successful deletion of Foxk2 (Supplementary Fig. 3d). Knockout of Foxk2 did not affect the body weight in male or female mice at 8 weeks of age (Supplementary Fig. 3e). The results of microCT showed that the bone mass (Fig. 2a) and the BV, BV/TV, and TB.N significantly reduced in *Osx-Cre;Foxk2*$^{fl/fl}$ mice compared to *Foxk2*$^{fl/fl}$ mice (Fig. 2b-2d), while the Tb.Sp was elevated (Fig. 2e). Biomechanical testing showed that loss of Foxk2 reduced the biomechanical properties of femur (Fig. 2f and 2g). We found that the trabecular bone area and number reduce in *Osx-Cre;Foxk2*$^{fl/fl}$ mice compared to *Foxk2*$^{fl/fl}$ mice by H&E staining (Fig. 2h). Dynamic histomorphometric analysis of calcein double labeling revealed that Foxk2 deletion reduced the bone formation activity, manifested as slower MAR and BFR (Fig. 2i-2k). In addition, OCN IHC staining revealed decreased osteoblast number in *Osx-Cre;Foxk2*$^{fl/fl}$ mice compared to *Foxk2*$^{fl/fl}$ mice (Fig. 2l and 2m). Trap staining revealed that deletion of Foxk2 had no effect on the number of osteoclasts (Fig. 2n and 2o).

Overexpression of Foxk2 in pre-osteoblasts increases bone mass of osteoporotic

mice

The positive role of Foxk2 in bone formation prompted us to explore its therapeutic potential in osteoporosis *in vivo*. We constructed an adeno-associated virus 9 (AAV9) that contained a pre-osteoblast-specific promoter (Osterix) to overexpress Foxk2 in pre-osteoblasts (AAV9-Osterix-Foxk2 (Supplementary Fig. 4a) according to our previously reported method[20]. We first validated the efficiency of viral infection in vitro, and the results showed that the upregulation of Foxk2 in osteoblasts was significantly higher than that in RAW cells and HL-1 cells (Supplementary Fig. 4b-4d), indicating satisfactory targeting.

Subsequently, adult female mice (8 weeks old) were induced ovariectomy (OVX) and administered AAV9-Osterix-Foxk2 (the group of OVX+Foxk2) or AAV9-Osterix-GFP (the group of OVX+GFP) via tail vein injection on the next day and their femora were collected of each mouse for bone morphologic and histologic analyses at 56 days after operation (Fig. 3a). The results of whole body and individual organ imaging showed that the expression of GFP was highest in the hindlimbs, modest in the liver and not detected in the heart, spleen, lung, and kidney (Fig. 3b), which was further confirmed by IF staining (Supplementary Fig. 4e). qPCR showed that the expression of Foxk2 decreased in the femurs of OVX mice, but treatment of AAV9-Osterix-Foxk2 significantly increased Foxk2 mRNA expression (Fig. 3c). In addition, AAV9-Osterix-Foxk2 improved Foxk2 expression in liver, while did not work in other tested organs (Supplementary Fig. 5a). H&E staining showed that no significant changes in histological features of the heart, liver, spleen, lung, and kidney in different groups (Supplementary Fig. 5b).

We found that Foxk2 overexpression could alleviate the loss of bone mass caused by ovariectomy, as indicated by the elevation of the BV, BV/TV, and TB.N and the decline of Tb.Sp (Fig. 3d-3h). Biomechanical testing also showed that overexpression of Foxk2 improved the biomechanical properties of femur, which were impaired by ovariectomy (Fig. 3i and 3j). Dynamic histomorphometric analysis of calcein double labeling revealed that Foxk2 promoted bone formation activity, characterized as increased MAR compared to OVX+GFP mice (Fig. 3k and 3l). The number of

osteoblasts decreased in ovariectomized mice, while overexpression of Foxk2 remarkably reversed this trend (Fig. 3m and 3o). Trap staining showed that the number of osteoclasts increased in ovariectomized mice (Fig. 3n and 3p), which is consistent with the activation of osteoclasts caused by estrogen deficiency. Treatment with AAV9-Osterix-Foxk2 had no significant effect on osteoclasts (Fig. 3n and 3p). These findings demonstrated that overexpression of Foxk2 in osteoblasts can partially rescue bone loss caused by osteoclast activation in animal model of osteopenia by ovarian resection.

Identification of Slc1a4 as a direct target of Foxk2

To investigate intrinsic mechanisms, we first performed RNA-seq of *Foxk2 KO* primary pre-osteoblasts. We identified a total of 1698 genes differentially expressed between *Foxk2 KO* and WT cell samples, including 1163 upregulated genes and 535 downregulated genes (Supplementary Fig. 6a). Pathway analysis suggested that genes related to ossification, skeletal system development, and Wnt signaling pathway were downregulated in *Foxk2 KO* cells compared with control (Fig. 4a), which further clarified the positive role of Foxk2 in osteoblast differentiation and bone formation. Next, considering that Foxk2 is a transcription factor, we performed Cleavage Under Targets and Tagmentation (CUT&Tag) assay of primary pre-osteoblasts to assess the DNA-binding profiles of Foxk2. We identified 773 genomic Foxk2 binding sites, of which 55.44% were localized on the promoter regions (Supplementary Fig. 6b). Pathway analysis of binding genes suggested that Foxk2 regulates cell metabolic process (Supplementary Fig. 6c), indicating that cell metabolism may be involve in Foxk2 regulated bone formation.

To gain insight into how Foxk2 regulates osteoblast differentiation, we sought to identify direct targets of Foxk2 among the differentially expressed genes that responded to loss of Foxk2. Among the downregulated genes in our RNA-seq data (total 535 genes) and genes directly targeted to the promoter region by Foxk2 protein (total 420 genes), 6 of which are overlapping (Fig. 4b). We focused on the overlapping candidate genes, and the RNA-seq data showed that deletion of Foxk2 significantly suppressed their expression, which was visualized through heatmap (Fig. 4c) and further confirmed by qPCR (Supplementary Fig. 6d). IGV visual analysis exhibited promoter region of

candidate genes, which were targeted by FOXK2 protein (Fig. 4d). To further examine whether candidate genes work as Foxk2 in osteoblast differentiation, we applied siRNA to knock down each gene in primary pre-osteoblasts. qPCR showed that each siRNA could knock down the corresponding candidate gene, but only knocking down Slc1a4 can inhibit osteoblast differentiation as Foxk2 deletion, characterized as decreased expression of osteogenic markers (Runx2, Osterix, Col1a1 and Alp) (Fig. 4e-4j). Furthermore, cells treated with siSlc1a4 displayed significant inhibition of ALP and ARS staining, while other 5 candidate genes did not work (Fig. 4k and 4l). Through these selection criteria, we were able to narrow down to Slc1a4 as the downstream target of Foxk2. To validate this finding, we performed qPCR after chromatin immunoprecipitation (ChIP) and found that FOXK2 protein bound to Slc1a4 promoter (Fig. 4m). Knocking out Foxk2 inhibited the expression of SlC1A4 protein in primary pre-osteoblasts (Fig. 4n). The expression of SlC1A4 increased during osteogenic differentiation (Fig. 4o), which coincides with the trend of FOXK2 expression (Supplementary Fig. 2b). And knockdown of Slc1a4 in pre-osteoblasts decreased the expression of RUNX2, OSTERIX, COL1A1 and ALP protein levels (Fig. 4p). These data collectively demonstrate that Slc1a4 is a downstream target of Foxk2 in regulating osteoblast differentiation and bone formation.

Knocking out of Slc1a4 in Pre-osteoblasts suppresses bone formation

To investigate the role of Slc1a4 in bone formation *in vivo*, the *Osx-cre* transgenic mice were mated with *Slc1a4*$^{fl/fl}$ mice to deplete Slc1a4 from committed osteoblast progenitors (Supplementary Fig. S7A). IHC staining revealed the successful deletion of Slc1a4, which was further confirmed by qPCR (Supplementary Fig. 7b and 7c). Male and female *Osx-cre;Slc1a4*$^{fl/fl}$ mice at 8 weeks of age were smaller and lighter than their *Slc1a4*$^{fl/fl}$ littermates (Supplementary Fig. 7d and 7e). We found that deletion of Slc1a4 exhibited lower bone mass through analyzing femur metaphysis with microCT compared to control, manifested as decreased BV, BV/TV, and TB.N with increased Tb.Sp (Fig. 5a-5e). Biomechanical testing showed that loss of Slc1a4 impaired the biomechanical properties of femur (Fig. 5f and 5g). H&E staining showed that the trabecular bone area and number reduced in *Osx-Cre;Slc1a4*$^{fl/fl}$ mice compared to

Slc1a4$^{fl/fl}$ mice (Fig. 5h). Dynamic histomorphometric analysis of calcein double labeling revealed that Slc1a4 deletion reduced the bone formation activity, indicted by slower MAR and BFR (Fig. 5i-5k). In addition, we found that the number of osteoblasts decreased in *Osx-Cre;Slc1a4*$^{fl/fl}$ mice compared to *Slc1a4*$^{fl/fl}$ mice (Fig. 5l and 5m) and deletion of Slc1a4 had no effect on the number of osteoclasts (Fig. 5n and 5o).

Slc1a4 function downstream of Foxk2 in osteoblast differentiation and bone formation

We sought to determine whether a Foxk2/Slc1a4 axis existed in regulating osteoblast differentiation and bone formation. Because deletion of Foxk2 and loss of Slc1a4 resulted in analogous phenotypes, we asked if overexpressing Slc1a4 could reverse the attenuation of osteoblast differentiation and bone formation owing to the loss of Foxk2. First, we overexpressed Slc1a4 in Foxk2 knockout primary pre-osteoblasts using plasmids and found that Slc1a4 overexpression could increase expression of osteogenic marker genes (Supplementary Fig. 8b-8e) and ALP and ARS staining (Supplementary Fig. 8f). Furthermore, overexpression of Slc1a4 could restore the impaired osteoblast differentiation caused by Foxk2 deletion, manifested as elevation of expression of osteogenic marker genes, ALP and ARS staining (Supplementary Fig. 8b-8f).

Next, we overexpressed Slc1a4 in postnatal day 1 *Osx-Cre;Foxk2*$^{fl/fl}$ mice with AAV9 via subcutaneous injection of AAV9-Osterix-Slc1a4 and harvested the femurs of each mouse for bone morphologic and histologic analyses at postnatal day 56 (Fig. 6a). qPCR showed that the expression of Foxk2 and Slc1a4 decreased in *Osx-Cre;Foxk2*$^{fl/fl}$ mice compared to *Foxk2*$^{fl/fl}$ mice (Supplementary Fig. 9a and 9b) and treatment with AAV9-Osterix-Slc1a4 significantly increased Slc1a4 gene expression (Supplementary Fig. 9b). MicroCT analysis of the femur metaphysis showed recovered bone mass in the treated *Osx-Cre;Foxk2*$^{fl/fl}$ mice, as shown by recovered skeletal parameters, including BV/TV, TB.N, and Tb.Sp (Fig. 6b-6e). Biomechanical testing revealed that overexpression of Slc1a4 restored the impaired biomechanical properties in the treated *Osx-Cre;Foxk2*$^{fl/fl}$ mice (Fig. 6f and Supplementary Fig. 9c). H&E staining validated the restored trabecular bone area and number in the treated *Osx-Cre;Foxk2*$^{fl/fl}$ mice (Fig.

6g and Supplementary Fig. 9d). The treated *Osx-Cre;Foxk2*$^{fl/fl}$ mice also showed recovered bone formation activity, manifested as elevated MAR and BFR (Fig. 6h-6j and Supplementary Fig. 9g). Increased number of osteoblast further confirmed restored bone formation in the treated *Osx-Cre;Foxk2*$^{fl/fl}$ mice (Fig. 6k and 6l). Trap staining showed that there was no significant change in the number of osteoclasts among the groups (Supplementary Fig. 9e and 9f).

The above data thus indicate that Slc1a4 functions to mediate, at least in part, the effect of Foxk2 in osteoblast differentiation and bone formation.

Foxk2/Slc1a4 promotes glutamine-dependent energy metabolism of osteoblast

Considering that Slc1a4 encodes a neutral amino acid transporter[21], we sought to explore whether amino acid metabolism is involved in Foxk2 regulated osteoblast differentiation. Amino acid metabolomics revealed that overexpression of Slc1a4 could restore the decrease of intracellular glutamine, glutamate and aspartate caused by deletion of Foxk2 (Fig. 7a and 7b, Supplementary Fig. 10a). Because previous studies have shown that glutamine metabolism plays a critical role in osteoblast differentiation and bone formation[8, 9], we focused on glutamine metabolism. In order to further validate the effect of Foxk2/Slc1a4 axis on glutamine metabolism, we used stable isotopically labeled glutamine to trace the metabolic fate of glutamine. Briefly, pre-osteoblasts were cultured in the presence of $^{13}C_5$-glutamine for 3 days and the contribution of glutamine-derived carbon to downstream metabolites was determined by measuring the mass isotope-labeling pattern (Fig. 7c). As expected, a significant amount of glutamate was derived from glutamine and glutamine carbon contributed to tricarboxylic acid (TCA) cycle intermediates (Fig. 7d-7h, Supplementary Fig. 10b and 10c). Deletion of Foxk2 impaired glutamine contributed to glutamate and TCA cycle intermediates, which could be recovered by overexpression of Slc1a4 (Fig. 7d-7h, Supplementary Fig. 10b and 10c). As previously reports, glutamine is converted into α-KG and enters the TCA cycle for mitochondrial energy production to drive multiple cellular physiological function[22]. These above findings suggest that deletion of Foxk2 may suppress osteoblast differentiation by reducing α-KG formation and affect energy metabolism in the TCA cycle through regulating Slc1a4. Then, we found that Foxk2 deletion resulted in

reduced mitochondrial oxygen consumption rate (OCR) during both basal and maximal respiration (Supplementary Fig. 10d-10f), and eventually led to reduced ATP production (Supplementary Fig. 10g and 10h). Overexpression of Slc1a4 restored impaired mitochondrial OCR and ATP production caused by Foxk2 deletion (Fig. 7i-7l). In addition, α-KG supplementation could reverse the suppressed osteoblast differentiation caused by loss of Foxk2, manifested as elevated expression of osteogenic markers, ALP and ARS staining (Fig. 7m-7r).

Collectively, our data demonstrate that Slc1a4 are functionally essential targets of Foxk2, and glutamine-dependent energy metabolism contributes to the overall function of Foxk2/Slc1a4 axis in osteoblast differentiation (Fig. 7s).

Discussion

Exploring the intrinsic mechanisms of regulating bone formation and searching for targets to promote osteogenesis remain crucial for improving the prevention and treatment of osteoporosis. Here, we report that Foxk2 plays a pivotal role in osteoblast differentiation and bone formation. Knockout of Foxk2 in pre-osteoblasts hindered osteoblast differentiation and bone formation. Overexpression of Foxk2 in pre-osteoblasts attenuated bone mass loss caused by ovariectomy. Mechanistically, we identified Slc1a4 as a downstream target of Foxk2 in regulating osteoblast differentiation and bone formation, which in turn promoted glutamine metabolism during osteoblast differentiation. Overexpression of Slc1a4 in pre-osteoblasts could alleviate the impairment of osteoblast differentiation and bone formation caused by knockout of Foxk2. Together, our study indicated that Foxk2 acts as a critical manipulator of osteoblast differentiation and bone formation, by regulating glutamine metabolism in osteoblast.

Foxk2 is one of the two members of the Foxk family, which is involved in various biological processes[23]. Numerous studies have shown that Foxk2 plays a crucial regulatory role in various types of cancer[14-16]. Our previous study revealed that Foxk1, as an important paralog of Foxk2, promotes osteoblast differentiation and bone formation by enhancing glycolysis in osteoblasts[20], which drive us to explore the role of Foxk2 in bone formation. We generated Foxk2 knockout mice with global deletions

and found that deletion of Foxk2 resulted in bone mass loss caused by impaired bone formation activity and suppression of osteoblast differentiation. Knocking out Foxk2 in pre-osteoblasts further confirmed the positive effect of Foxk2 on osteoblast differentiation and bone formation. A recent study showed that Foxk2 plays an essential role in skeletal muscle development and mitochondrial homeostasis and acts as a novel pathogenic gene for congenital myopathy[24]. In addition, Foxk2 promotes adaptogenic differentiation by regulating PPAR-γ[25]. To our best knowledge, this is the first report revealing the roles of Foxk2 in osteoblast differentiation and bone formation. More importantly, our results showed that overexpression of Foxk2 in pre-osteoblasts by a pre-osteoblast-specific promoter (Osterix) modified AAV9[20], could effectively prevent bone loss caused by ovariectomy. Our findings provide potential targets for the prevention and treatment of osteoporosis.

Slc1a4, as a neutral amino acid transporter, plays a vital role in neurodevelopmental, neurodegenerative disorders[21, 26], regulating blood-brain barrier[27], and cancer progression[28-30]. In this study, we identified Slc1a4 as a Foxk2 direct target in osteoblast differentiation and bone formation through conjoint analysis of the data of RNA-seq and CUT&Tag. We found that FOXK2 protein could bide to the promoter region of Slc1a4 gene and deletion of Foxk2 suppressed the expression of Slc1a4 in osteoblast. Loss of Slc1a4 in pre-osteoblasts caused repression of osteoblast differentiation *in vitro*, as well as bone loss and impaired bone formation activity in mice, which further confirms its function in bone biology. Notably, overexpression of Slc1a4 in pre-osteoblasts could alleviate the decreased bone mass and bone formation activity caused by deletion of Foxk2 in mice. Thus, our findings demonstrated that Foxk2/Slc1a4 axis plays a vital role in osteoblast differentiation and bone formation.

The function of glutamine in osteoblasts has been extensively explored. Deprivation of glutamine hinders osteoblast differentiation and bone formation[8, 9]. Glutamine metabolism is involved in the process of bone formation promoted by recognized osteogenic factors (PTH and WNT3A)[9], and is related to skeletal stem cells specification[31]. Slc1a4, as the downstream of Foxk2, facilitates the transport of neutral amino acids, including serine, alanine, and cysteine, across the cell membrane[26]. A more

recent study revealed that Slc1a4 acts as a glutamine transporter in stomach cancer[32]. We found that the content of intracellular glutamine could be regulated by Foxk2/Slc1a4 axis, which indicate that Slc1a4 can transport glutamine in osteoblasts under the regulation of Foxk2. And the subsequent isotopic labeling experiment further confirmed that Foxk2/Slc1a4 plays a crucial role in regulating glutamine metabolism. Interestingly, our results demonstrated that Foxk2/Slc1a4 tends to mainly manipulate the TCA cycle intermediates contributed by glutamine, which indicated mitochondrial respiration may be perturbed. This hypothesis was further verified by Seahorse XF24 assay, namely overexpression of Slc1a4 could alleviate the inhibition of mitochondrial respiration caused by knockout of Foxk2. And we found that supplementation of α-KG, a key intermediate of glutamine entering the TCA cycle, can reverse the inhibition of osteoblast differentiation caused by Foxk2 deletion. Glutamine dependent energy metabolism plays a vital role in various pathophysiological processes[22, 32, 33], which is consistent with our findings. Thus, the identification of metabolic regulators, such as Foxk2/Slc1a4, may provide potential therapeutic options for prevention and treatment of osteoporosis.

Methods

Mice

All experimental procedures were approved by Animal Ethics Review Committee of Shenzhen People's Hospital and all procedural interventions strictly adhered to its stipulated guidelines. All mice maintained a 12-hour light/dark cycle and were free to eat and drink. According to animal care guidelines, the sample size of animals is minimized. Mice were randomly assigned to the experimental group. WT C57BL/6J mice were obtained from BIOTECHNOLOGY CO., LTD. (Beijing, China). *Foxk2 KO* mice were obtained from Professor Yu Nie of Fuwai Hospital, Chinese Academy of Medical Sciences. $Foxk2^{fl/+}$ and $slc1a4^{fl/+}$ mice were purchased from Cyagen Biosciences (Suzhou, China). *Osterix-Cre* mice were purchased from BIOCYTOGEN (Shanghai, China). To generate *Osx-cre;*$Foxk2^{fl/fl}$ and *Osx-cre;*$Slc1a4^{fl/fl}$ conditional knockout mice, $Foxk2^{fl/+}$ and $Slc1a4^{fl/+}$ mice were crossed for over three generations with *Osterix-Cre* mice. Tail genome DNA is used to identify genotypes through PCR

amplification. The genotype identification primers for Foxk2 knockout, *Foxk2*$^{fl/+}$, *slc1a4*$^{fl/+}$ allele and Osterix-Cre transgenic mice are listed in Supplementary Table S1. All mice were propagated and raised in Specific pathogen free facilities.

AAV9 construction and injection in mice

Adeno-associated virus-9 (AAV9) was used as a vector to overexpressed Foxk2 or slc1a4 in mice. The AAV9 vector was designed and synthesized by WZ Biosciences Co., Ltd. (Shangdong, China), and specifically targets pre-osteoblasts lineage cells by modifying the pre-osteoblast specific promoter osterix.

As previously reported, the OVX model was constructed by removing bilateral ovaries via a dorsal approach in 8-week-old mice[34]. The sham surgery was performed using the same method until both ovaries are exposed. 4×10^{11} GC AAV9 were diluted with PBS to 100 μl and inject it into each mouse via tail vein 1 day after surgery. Mice were sacrificed at 56 days after surgery for further analysis. Grouping as follows: The sham surgical mice injected with AAV9-Osterix-GFP (sham); OVX mice injected with AAV9-Osterix-GFP (OVX+GFP); OVX mice injected with AAV9-Osterix-Foxk2 (OVX+Foxk2). 100 μl PBS was injected into the tail vein as the control group, and GFP expression was imaged in both whole body and individual organs at 2 weeks after injection.

To investigate whether Slc1a4 is involved in Foxk2 regulated bone formation *in vivo*, 2×10^{11} GC AAV9 were diluted with PBS to 10 μl and inject into postnatal day 1 mice via subcutaneous injection. Mice were sacrificed at postnatal day 56 days for further analysis. Grouping as follows: *Foxk2*$^{fl/fl}$ mice injected with AAV9-Osterix-GFP (Foxk2$^{fl/fl}$+GFP); *Foxk2*$^{fl/fl}$ mice injected with AAV9-Osterix-Slc1a4 (Foxk2$^{fl/fl}$+Slc1a4); *Osx-Cre;Foxk2*$^{fl/fl}$ mice injected with AAV9-Osterix-GFP (Osx-Cre;Foxk2$^{fl/fl}$+GFP); *Osx-Cre;Foxk2*$^{fl/fl}$ mice injected with AAV9-Osterix-Slc1a4 (Osx-Cre;Foxk2$^{fl/fl}$+ Slc1a4).

MicroCT

The collected right femurs of the mouse were fixed with 4% paraformaldehyde for 48 hours at 4 °C. and scanned with a MicroCT system (SkyScan 1276, Bruker, Belgium) at 80 kVp, 100 μA, exposure time 926 ms, and 20 μm pixels. Two-dimensional images

of the distal femur and three-dimensional images of the distal femoral trabecular bone were reconstructed using NRecon software. The volume of interest (VOI) of femurs was defined as a cylindrical area at the distal region of the growth plate. Bone volume was calculated within the delimited VOI. The bone volume/tissue volume ratio (BV/TV), bone volume (BV), trabecular number (Tb.N) and trabecular separation (Tb.Sp) were analyzed.

Bone biomechanical properties

The biomechanical properties were tested using three-point bending mechanical strength devices (AG-IS, Shimadzu, Japan) as previous described[35]. Briefly, the left femurs of the mouse were collected and cleaned of adherent tissue. A three-point bending test was performed on the mid femur wrapped in gauze soaked in saline solution. Adjust the compression speed of the femur to 1mm/min at two points 6mm apart. The biomechanical data were analyzed to determine the max bending strength, and elastic modulus.

Calcein double labeling

To investigate the dynamic osteogenic activity, Calcein (20 mg/kg; Sigma-Aldrich, C0875, Missouri, USA) was injected to mice at 9 days and 3 days before sacrifice. Dehydrate the right femur with a 20% sucrose solution and use a Leica SM2500E microtome (Leica Microsystems, Wetzlar Germany) to freeze slice it at a thickness of 10 μm to obtain anterior sections of trabecular bone. Capture fluorescence images using confocal microscopy (Leica, Wetzlar, Germany). Then mineral apposition rate (MAR) and bone formation rate (BFR) were analyzed by ImageJ software (NIH, USA).

Immunohistochemical staining and immunofluorescence.

The bone tissue was fixed with 4% paraformaldehyde for 48 hours, and then decalcified with 15% EDTA. The decalcified specimens were embedded in paraffin and sliced to 5-μm-thick sections using a microtome ((Leica, Wetzlar, Germany). Then sections were de-waxed and rehydrated, and used for subsequent H&E staining, IHC staining, IF staining and Trap staining. IHC staining and IF staining were performed according to the protocol. Briefly, after incubating primary antibody at 4℃ overnight, incubate secondary antibodies at room temperature for 1 hour. Then take photos for

analysis. OCN IHC staining is used for OCN positive osteoblast counting as previous described[36]. Count the number of osteoblasts on the surface of trabecular bone in the entire region of interest, and then normalize the data to the number of osteoblasts per millimeter of trabecular surface circumference. Trap staining is used for osteoclast counting as previous described[36]. IHC and Trap staining images were captured using a microscope (TS2-S-SM; Nikon, Tokyo, Japan) in bright field. Fluorescence images were Obtained using an inverted fluorescence microscope (Leica image analysis system, Q500MC). Antibody against FOXK2 (NBP1-87700) was obtained from Novus (Colorado, USA). Antibody against SLC1A4 (BA3476) was obtained from Boster (Wuhan, China). Antibody against GFP (ab290) was obtained from abcam (Cambridge, England). Antibodies against OCN (sc-390877) and OSTERIX (sc-393325) were obtained from santa cruz biotechnology (California, USA). Anti-rabbit (A-11008, A-11012, 1:400) and anti-mouse (A-11005, A-11001) secondary antibody were obtained from Invitrogen (California, USA). TRAP staining kit (387A) was obtained from Sigma Aldrich (Missouri, USA).

Cell culture and osteoblast differentiation

The primary pre-osteoblasts were isolated from the mouse calvaria of 1 to 3-day-old pups as previous described[20]. Briefly, cut the collected mouse calvarias into fragments and incubate with 2.5% trypsin (Gibco, 25200072, New York, USA) at 37 °C for 10 minutes with gentle shaking. Discard the supernatant and incubate with 0.2% type 1 collagenase (Biyotime, ST2294-100mg, Shanghai, China) at 37 °C for 30 minutes with gentle shaking. Discard the supernatant again and continue incubating with 0.2% type 1 collagenase at 37 °C for 60 minutes with gentle shaking. Then supernatant was Collected and centrifuged at 300g for 5 minutes. Resuspend the cell pellet using α-MEM (Gibco, 12571063) with 10% fetal bovine serum (Gibco, 10099141 C) and incubate overnight in a cell culture incubator. The next day, the cell culture medium was replaced with fresh medium, non-adherent cells in the supernatant was discarded.

For all cell experiments, the primary pre-osteoblasts were incubated with osteogenic induction medium, containing 10 mM b-glycerol phosphate (Sigma-Aldrich,

G9422) and 50 ug/ml ascorbic acid (Sigma-Aldrich, A4544). The small interfering RNAs (Table S2) and plasmid were obtained from Hanbio Co. Ltd (Shanghai, China). The small interfering RNAs and plasmid were transfected into the primary pre-osteoblasts after reaching ~80-90% confluency using Lipofectamine 3000 (Invitrogen, 11668027, California, USA) in accordance with the manufacturer's instructions.

Western blotting

The treated cells were washed with pre-chilled PBS and lysed with RIPA (Biyotime, P0013B, Shanghai, China) buffer containing protease inhibitors (Biyotime, P1005) using appropriate power ultrasound. And the bone tissues were pulverized in RIPA lysis buffer containing protease inhibitors. The concentration of protein was analyzed with BCA kit (Biyotime, P0009) and 20 μg protein was run on 12-14% SDS-PAGE gels (Yeasen Biotechnology, 36249ES10, Shanghai, China). Then the gels containing protein were transferred to PVDF membranes (Millipore, IPVH00005, Massachusetts, USA). After blocked with TBST containing 5% dried skimmed milk, PVDF membranes were incubated primary antibody overnight in 4℃. PVDF membranes were incubated with second antibody in room temperature for 1hour and then visualized using SuperSignal™ West Pico PLUS Chemiluminescent Substrate Reagent (Thermo Fisher Scientific, 34580 Massachusetts, USA). Primary antibodies: anti-FOXK2 (1:1000, Novus, NBP1-87700, Colorado, USA), anti-SLC1A4 (1:500, Boster, BA3476, Wuhan, China), anti-RUNX2 (1:500, Proteintech, 20700-1-AP, Wuhan, China), anti-OSTERIX (sc-393325, 1:500), anti-ALP (1:500, Proteintech, 60294-1-Ig), anti-COL1A1 (1:500, Boster, BA0325), anti-β-ACTIN (1:1000, Abways, Shanghai, China), anti-GAPDH (1:1000, 30202ES60, Yeasen Biotechnology, Shanghai, China) and anti-β-Tubulin (1:1000, Proteintech, 10094-1-AP). Secondary antibodies: HRP anti-rabbit (Proteintech, RGAR001, 1:5000) and HRP anti-mouse (Proteintech, RGAM001, 1:5000).

qPCR

The total RNA from cells were extracted with the RNeasy kit (Qiagen, 74104, Hilden, Germany) and bone tissues with TRIzol reagent (Invitrogen, 15596018CN), as the manufacturers' instructions. The concentration of RNA was analyzed by a Nano-Drop

ND-2000 spectrophotometer (Thermo Fisher Scientific). The Prime Script™ Reverse Transcript Master Mix (TaKaRa Bio, RR037A, Otsu, Japan) was applied to perform Reverse transcription. qPCR was performed on a StepOnePlus Real-Time PCR system (Applied Biosystems, Waltham, USA). The relative mRNA concentrations were determined by the approach of $2^{-\Delta\Delta Ct}$ and normalized to that of β-actin. The primers used for qPCR are listed in Table S3.

ALP and Alizarin red staining

ALP staining was performed after 7 days of cell osteogenic induction, and Alizarin red staining (ARS) was performed after 14 days of induction. The treated cells were washed twice with room temperature PBS, and then incubated with ALP (Beyotime, P0321S) or ARS (Beyotime, C0140-100ml) reagents at room temperature for 30 minutes. After washing three times, the stained cells were photographed by light microscopy (TS2-S-SM, Nikon, Japan).

RNA-seq and data analysis

Wild-type and Foxk2 KO primary pre-osteoblasts were undergone osteogenic induction for 3 days and then performed extraction of total RNA. Total amounts and integrity of RNA were assessed using the RNA Nano 6000 Assay Kit of the Bioanalyzer 2100 system (Agilent Technologies, CA, USA). The RNA samples being used is required an A260/A280 ratio of 1.9–2.0 and an RNA integrity number (RIN) > 9.5. After the library is qualified, then being sequenced by the Illumina NovaSeq 6000 (San Diego, CA, USA) at Novogene Science and Technology Co., Ltd (Beijing, China). The image data measured by the high-throughput sequencer are converted into sequence data (reads) by CASAVA base recognition. Next, clean the raw data to ensure high-quality data for analysis. Clean data was mapped with the reference genome using Hisat2 (v2.0.5). FeatureCounts (1.5.0-p3) are used to calculate the readings mapped to each gene, and then calculate the FPKM of each gene based on its length. Differential expression of genes between groups (Padj≤0.05 & $|\log2^{(foldchange)}|\geq1$) were analyzed by DESeq2 software (1.20.0). Gene Ontology (GO) analysis of genes with differentially downregulated expression were performed using the clusterProfiler R package (3.8.1). GO terms with corrected Pvalue less than 0.05 were considered significantly enriched

by differential expressed genes.

CUT&Tag

Primary pre-osteoblasts were overexpressed Foxk2 using adenovirus and cultured in osteogenic induction for 3 days. The C-terminal of adenovirus vector contains triple Flag-tag (3×Flag), which provided attachment sites for subsequent experiments. Then treated cells were harvested to perform CUT&Tag using a Hyperactive Universal CUT&Tag Assay Kit for Illumina (Vazyme Biotechnolegy, TD903-01, Nanjing, China) according to the manufacturer's protocol. Briefly, cells were resuspended with 100 μl wash buffer and incubated with activated ConA Beads for 10 min at room temperature. Precipitation obtained by instantaneous centrifugation was resuspended with 50 μl precooled antibody buffer containing 1 μg anti-FLAG antibody (Sigma-Aldrich, F7425, St. Louis, Missouri, USA) and incubated in 4℃ overnight with rotation. The supernatant was discarded and sediment incubated with secondary antibody for 60 min at room temperature. Sediment incubated with 100 μl Dig-300 Buffer containing 2 μl pA/G-Tnp for 60 min, and then made fragmentation of chromatin by incubating with 50 μl Dig-300 Buffer containing 10 μl 5×TTBL for 60 min at 37°C. After undergoing protein lysis with proteinase K and several washes, DNA was eluted with 22 μl sterilized ultrapure water. The amplified library was purified with the AMPure beads and assessed on the Agilent Bioanalyzer 2100 system. Finally, the library preparation was sequenced at Novogene Science and Technology Co., Ltd. and 150 bp paired-end reads were generated. Raw data of fastq format were firstly processed using fastp (version 2.1.0) to clean up. Clean reads were aligned to the reference genome using BWA (V0.7.12) mem. All peak calling was performed with MACS2 (version 2.1.0) and peaks with q-value threshold of 0.05 was used for all data sets. Peaks were adjusted to the same size (500 bp) centered peak summits and motif discoveries of these loci sequences were performed using findMotifsGenome.pl program in HOMER v4.11. Chip seeker was used to confirm Peak-related genes. Gene Ontology (GO) enrichment analysis was performed to identify the function enrichment results and was implemented by the GOseq R package, in which gene length bias was corrected. GO terms with corrected P-value less than 0.05 were considered significantly enriched by

peak-related genes.

ChIP assay

Primary pre-osteoblasts were overexpressed Foxk2 using adenovirus and perform ChIP using a SimpleChIP® Enzymatic Chromatin IP Kit (Cell Signaling Technology, 9003, Massachusetts, USA) after osteogenic induction for 3 days according to the manufacturer's protocol. In brief, protein and DNA were crosslinked by 37% formaldehyde solution. The chromatin was broken to 200-1000bp with enzymes and ultrasound and tested by PCR electrophoresis. Chromatin fragments were incubated with 1 μg primary antibody of anti- FLAG antibody (Sigma-Aldrich, F7425) or anti-IgG (Cell Signaling Technology, 9003) at 4°C overnight with rotation. DNA samples were precipitated with magnetic beads and then undergone uncoupling and purification. The purified DNA sample was quantified by qPCR with specific primers (Table S4).

Amino acid metabolomics

Primary pre-osteoblasts were isolated from calvaria of WT and *Foxk2 KO* neonatal mice, and Slc1a4 was overexpressed in *Foxk2 KO* cells using plasmids. Experimental groups: WT+oeNC (WT cells added control plasmids); Foxk2 KO+oeNC (*Foxk2 KO* cells added control plasmids); Foxk2 KO+oeSlc1a4 (*Foxk2 KO* cells added Slc1a4 overexpression plasmids). Cells were harvested to quantify amino acid using UPLC-MS/MS（ACQUITY UPLC-Xevo TQS, Waters Corp., Milford, MA, USA）at Metabo-Profile Biotechnology Co., Ltd. (Shanghai, China) after inducing osteogenesis for 3 days. The raw data obtained from UPLC-MS/MS were processed by MassLynx software (v4.1, Waters, Milford, MA, USA). Then the peaks for each metabolite were extracted, integrated, and quantified.

Glutamine metabolic flux detection

Primary pre-osteoblasts were isolated from calvaria of WT and *Foxk2 KO* neonatal mice, and Slc1a4 was overexpressed in *Foxk2 KO* cells using plasmids. Experimental groups: WT+oeNC (WT cells added control plasmids); Foxk2 KO+oeNC (*Foxk2 KO* cells added control plasmids); Foxk2 KO+oeSlc1a4 (*Foxk2 KO* cells added Slc1a4 overexpression plasmids). After 3 days of osteogenic induction, each group of cells was

incubated with $^{13}C_5$-glutamine (Sigma-Aldrich, 605166) for 24 hours. Cells were harvested to detect isotope labeled metabolites uses a liquid platform (ACQUITY-I UPLC /Xevo TQS, Waters Corp..). The raw data generated by UPLC-TQMS will be extracted, integrated, identified, and quantitatively analyzed for each metabolite using Waters' MassLynx software (v4.1, Waters, Milford, MA, USA).

Measurement of oxygen consumption rate and ATP

Oxygen Consumption Rate (OCR) were determined by XF24 Extracellular Flux Analyzer (Seahorse Bioscience, Maine, USA). Briefly, 70000 primary pre-osteoblasts were seeded on a poly-Llysine-coated XF24 V7 microplate (Seahorse Bioscience) and then performed corresponding interventions as described in the results. Then, the plates were texted according to the instructions of the XF24 Cell Mito Stress Test Kit (103015-100). Data were analyzed with the XFe Wave Software and normalized to the cell number.

Statistical analysis

Statistical analysis was performed by Prism 8 (GraphPad software). All data are presented as the mean ± standard error of the mean (SEM). Unpaired two-tailed Student's t-test was applied to determine the statistical significance between two groups. One-way ANOVA followed by Tukey's multiple comparisons test or two- ANOVA followed by Sidak's multiple comparisons was used to determine the statistical significance of multiple groups comparison. $P<0.05$ is considered statistically significant.

Reference

1. Wang Y*, et al.* Alpha-ketoglutarate ameliorates age-related osteoporosis via regulating histone methylations. *Nat Commun* **11**, 5596 (2020).
2. Fukuda M*, et al.* SIRT7 has a critical role in bone formation by regulating lysine acylation of SP7/Osterix. *Nat Commun* **9**, 2833 (2018).
3. Borumandi F, Aghaloo T, Cascarini L, Gaggl A, Fasanmade K. Anti-resorptive Drugs and their Impact on Maxillofacial Bone among Cancer Patients. *Anticancer Agents Med Chem* **15**, 736-743 (2015).
4. Reid IR, Billington EO. Drug therapy for osteoporosis in older adults. *Lancet* **399**, 1080-1092 (2022).
5. Yang Y-S*, et al.* Bone-targeting AAV-mediated silencing of Schnurri-3 prevents bone loss in osteoporosis. *Nat Commun* **10**, 2958 (2019).
6. Esen E, Long F. Aerobic glycolysis in osteoblasts. Curr Osteoporos Rep 12, 433-

438 (2014).
7. Ahmad M*, et al.* Inhibition of Cdk5 increases osteoblast differentiation and bone mass and improves fracture healing. *Bone Res* **10**, 33 (2022).
8. Brown PM, Hutchison JD, Crockett JC. Absence of glutamine supplementation prevents differentiation of murine calvarial osteoblasts to a mineralizing phenotype. Calcif Tissue Int 89, 472-482 (2011).
9. Stegen S, Devignes C-S, Torrekens S, Van Looveren R, Carmeliet P, Carmeliet G. Glutamine Metabolism in Osteoprogenitors Is Required for Bone Mass Accrual and PTH-Induced Bone Anabolism in Male Mice. *J Bone Miner Res* **36**, 604-616 (2020).
10. Cai D*, et al.* Foxk1 and Foxk2 promote cardiomyocyte proliferation and heart regeneration. *Nat Commun* **16**, 2877 (2025).
11. Bowman CJ, Ayer DE, Dynlacht BD. Foxk proteins repress the initiation of starvation-induced atrophy and autophagy programs. *Nat Cell Biol* **16**, 1202-1214 (2014).
12. Ji Z, Li Y, Liu SX, Sharrocks AD. The forkhead transcription factor FOXK2 premarks lineage-specific genes in human embryonic stem cells for activation during differentiation. *Nucleic Acids Res* **49**, 1345-1363 (2021).
13. Sukonina V*, et al.* FOXK1 and FOXK2 regulate aerobic glycolysis. *Nature* **566**, 279-283 (2019).
14. Zhang Y, Wang Y, Zhao G, Tanner EJ, Adli M, Matei D. FOXK2 promotes ovarian cancer stemness by regulating the unfolded protein response pathway. *J Clin Invest* **132**, (2022).
15. Yu Y*, et al.* FOXK2 amplification promotes breast cancer development and chemoresistance. *Cancer Lett* **597**, 217074 (2024).
16. Du F*, et al.* Forkhead box K2 promotes human colorectal cancer metastasis by upregulating ZEB1 and EGFR. *Theranostics* **9**, 3879-3902 (2019).
17. Sakaguchi M*, et al.* FoxK1 and FoxK2 in insulin regulation of cellular and mitochondrial metabolism. *Nat Commun* **10**, 1582 (2019).
18. Shan L*, et al.* FOXK2 facilitates the airway remodeling during chronic asthma by promoting glycolysis in a SIRT2-dependent manner. *FASEB J* **38**, e23756 (2024).
19. Li Y*, et al.* FOXK2 affects cancer cell response to chemotherapy by promoting nucleotide de novo synthesis. *Drug Resist Updat* **67**, 100926 (2023).
20. Liu C*, et al.* Foxk1 promotes bone formation through inducing aerobic glycolysis. *Cell Death Differ* **31**, 1650-1663 (2024).
21. Gu H-C*, et al.* Human urine stem cells protect against cyclophosphamide-induced premature ovarian failure by inhibiting SLC1A4-mediated outflux of intracellular serine in ovarian granulosa cells. *Cell Mol Biol Lett* **30**, 21 (2025).
22. Peng R*, et al.* IL-17 promotes osteoclast-induced bone loss by regulating glutamine-dependent energy metabolism. *Cell Death Dis* **15**, 111 (2024).
23. Ji Z, Donaldson IJ, Liu J, Hayes A, Zeef LAH, Sharrocks AD. The forkhead transcription factor FOXK2 promotes AP-1-mediated transcriptional regulation. Mol Cell Biol 32, 385-398 (2011).
24. Wu P*, et al.* FOXK2 in skeletal muscle development: a new pathogenic gene for congenital myopathy with ptosis. *EMBO Mol Med* **17**, 1599-1630 (2025).

25. Zhang S, *et al.* Foxk2 Enhances Adipogenic Differentiation by Relying on the Transcriptional Activation of Peroxisome Proliferator-Activated Receptor Gamma. *J Cell Mol Med* **29**, e70332 (2025).
26. Elazar D, Alvarez N, Drobeck S, Gunn TM. SLC1A4 and Serine Homeostasis: Implications for Neurodevelopmental and Neurodegenerative Disorders. *Int J Mol Sci* **26**, (2025).
27. Odeh M, *et al.* A new type of blood-brain barrier aminoacidopathy underlies metabolic microcephaly associated with SLC1A4 mutations. *Brain* **147**, 3874-3889 (2024).
28. Zhao J, *et al.* Skullcapflavone II Inhibits SLC1A4-Mediated L-Serine Uptake and Promotes Mitochondrial Damage in Gastric Cancer. *Adv Sci (Weinh)* **12**, e17225 (2025).
29. Zhang S, *et al.* NAT10-mediated mRNA N4-acetylcytidine reprograms serine metabolism to drive leukaemogenesis and stemness in acute myeloid leukaemia. *Nat Cell Biol* **26**, 2168-2182 (2024).
30. Chakraborty A, Patnaik J, Sinha A, Parida N, Parija T, Patnaik S. In silico analysis shows slc1a4 as a potential target of hsa-mir-133a for regulating glutamine metabolism in gastric cancer. *Int J Biol Macromol* **282**, 136974 (2024).
31. Yu Y, *et al.* Glutamine Metabolism Regulates Proliferation and Lineage Allocation in Skeletal Stem Cells. *Cell Metab* **29**, (2019).
32. Cai Y, *et al.* Glutamine Metabolism Promotes Renal Fibrosis through Regulation of Mitochondrial Energy Generation and Mitochondrial Fission. *Int J Biol Sci* **20**, (2024).
33. Weng H, *et al.* The m6A reader IGF2BP2 regulates glutamine metabolism and represents a therapeutic target in acute myeloid leukemia. *Cancer Cell* **40**, (2022).
34. Dong Y, *et al.* Blocking the cytohesin-2/ARF1 axis by SecinH3 ameliorates osteoclast-induced bone loss via attenuating JNK-mediated IRE1 endoribonuclease activity. *Pharmacol Res* **185**, 106513 (2022).
35. Yang Y-Y, *et al.* Lgr4 promotes aerobic glycolysis and differentiation in osteoblasts via the canonical Wnt/β-catenin pathway. *J Bone Miner Res* **36**, 1605-1620 (2021).
36. Liu J-H, *et al.* Extracellular Vesicles from Child Gut Microbiota Enter into Bone to Preserve Bone Mass and Strength. *Adv Sci (Weinh)* **8**, 2004831 (2021).

Acknowledgements

We would like to thank Professor Yu Nie of Fuwai Hospital, Chinese Academy of Medical Sciences, for providing the *Foxk2 KO* mice. This work was supported by the National Natural Science Foundation of China (82472413, 82272488, and 82500453), the National Key Research and Development Program (2023YFC2307003), the project (C2501018) from Shenzhen Medical Research Fund, Natural Science Foundation of Guangdong Province (2024A1515012790), and the projects (KCXFZ20240903093917023 and JCYJ20240813104125034) from Shenzhen Science and Technology Innovation Bureau, the Shenzhen People's Hospital Clinician Scientist Training 'Five Three' Plan Project (SYWGSJCYJ202302).

Conflict of Interest Statement

The authors declare no competing interests.

Author Contribution Statement

S.P. and H.L. designed and supervised the entire project. C.L., J.Z. and J.L. wrote the draft of this manuscript. C.L. and J.Z. performed most of the experiments. Z.W., K.Z., Y.X. and J.D. conducted partial experiments. C.L. and J.L. analyzed the data. All authors discussed the results and commented on the paper.

Ethics statement

The study was performed in accordance with the Declaration of Helsinki. All animal experimentation conducted in this investigation received approval from the Animal Ethics Review Committee of Shenzhen People's Hospital, and all procedural interventions strictly adhered to its stipulated guidelines.

Funding statement

This work was supported by the National Natural Science Foundation of China (82472413, 82272488, and 82500453), the National Key Research and Development

Program (2023YFC2307003), the project (C2501018) from Shenzhen Medical Research Fund, Natural Science Foundation of Guangdong Province (2024A1515012790), and the projects (KCXFZ20240903093917023 and JCYJ20240813104125034) from Shenzhen Science and Technology Innovation Bureau, the Shenzhen People's Hospital Clinician Scientist Training 'Five Three' Plan Project (SYWGSJCYJ202302).

Data availability

All data and material that support this study are available upon requests to the corresponding authors. The RNA-seq data generated in this study have been deposited in the GEO database under accession code GSE308107. The CUT&Tag data generated in this study have been deposited in the NCBI database under accession code PRJNA1406518. Source data are provided with this paper.

Figures and figure legends

Figure 1

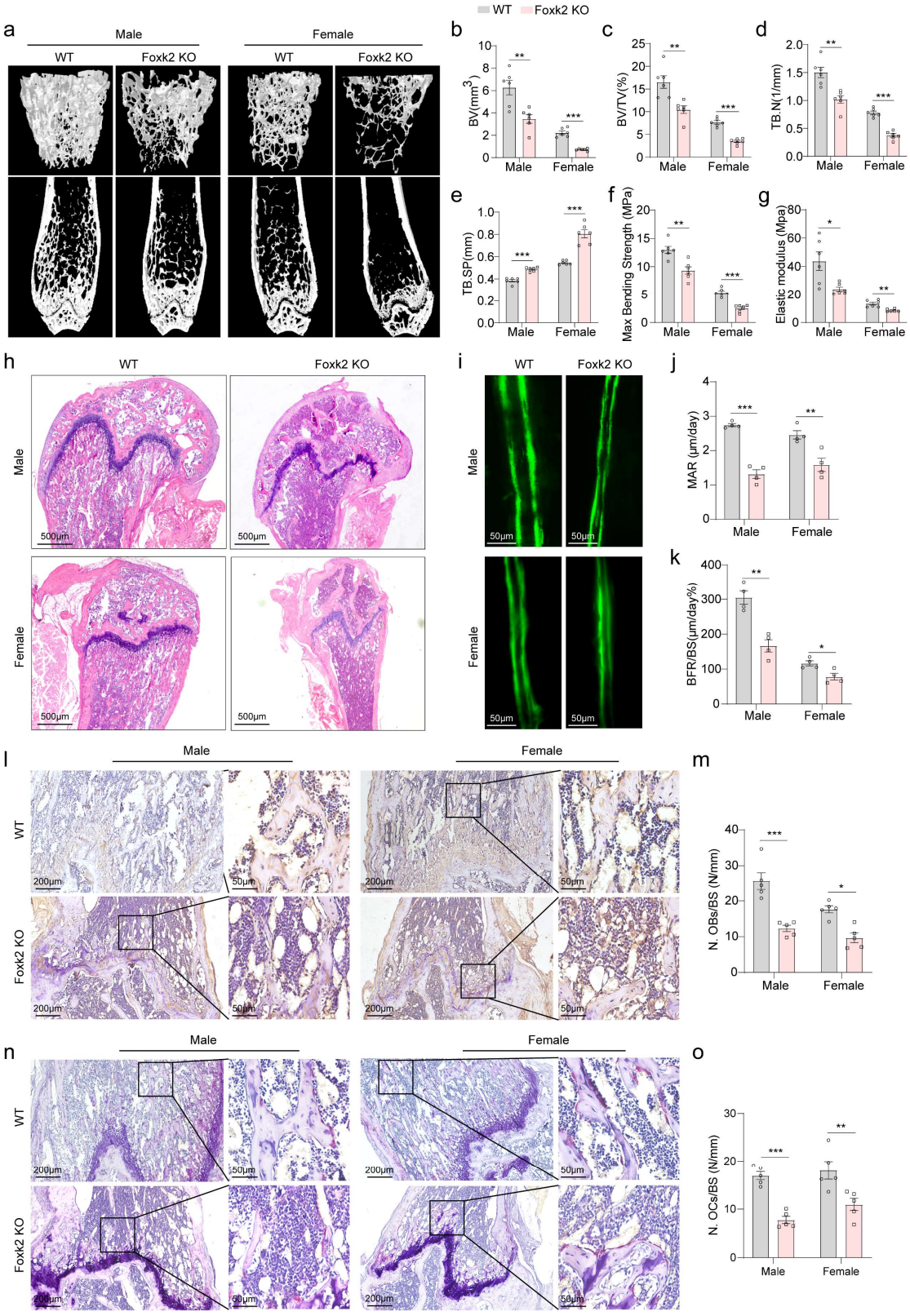


Figure 1. Deletion of Foxk2 decreased bone mass. (a) Representative images of microCT analysis of male and female *Foxk2 KO* and WT mice including two-

764 dimensional construction of distal femur and three-dimensional reconstruction of
765 trabecular bone of distal femur at 8 weeks old. (b-e) Quantitative microCT analyses of
766 the distal end of the femurs from male and female *Foxk2 KO* and WT mice at 8 weeks
767 old (*n=6*), including bone volume (BV) (b), bone volume/tissue volume ratio (BV/TV)
768 (c), trabecular number (TB.N) (d) and trabecular separation (Tb.Sp) (e). (f and g)
769 Quantitative analysis of biomechanics of the femurs from male and female *Foxk2 KO*
770 and WT mice at 8 weeks old (*n=6*), including maximum bending strength (f), and
771 elastic modulus (g). (h) H&E staining of the femurs from male and female *Foxk2 KO*
772 and WT mice at 8 weeks old. (i-k) Representative images (i) and quantitative analysis
773 of calcein double labeling, including mineral apposition rate (MAR) and bone
774 formation rate (BFR) (*n=4*). (l) Representative images of OCN IHC staining in male
775 and female WT and *Foxk2 KO* mice at 8 weeks old. (m) Quantification of OCN IHC
776 staining *(n=5)*. (n) Representative images of Trap staining in male and female WT and
777 *Foxk2 KO* mice at 8 weeks old. (o) Quantification of Trap staining (*n=5*). *$p < 0.05$,
778 **$p < 0.01$, ***$p < 0.001$.

Figure 2

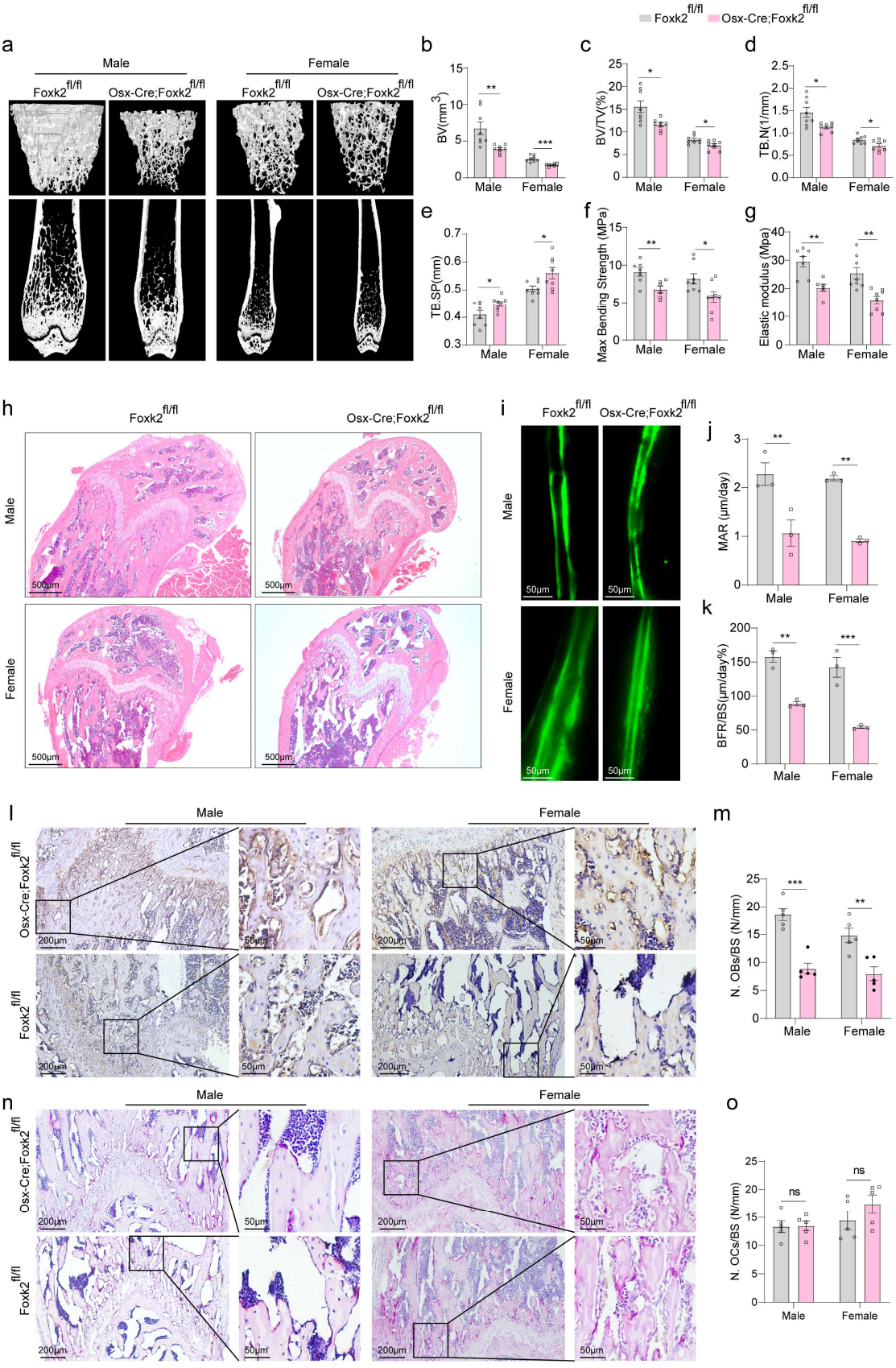


Figure 2. Loss of Foxk2 in Pre-osteoblasts causes reduced bone mass. (a)

Representative images of microCT analysis of male and female *Osx-Cre;Foxk2*$^{fl/fl}$ and *Foxk2*$^{fl/fl}$ mice including two-dimensional construction of distal femur and three-dimensional reconstruction of trabecular bone of distal femur at 8 weeks old. (b-e) Quantitative microCT analyses of the distal end of the femurs from male and female *Osx-Cre;Foxk2*$^{fl/fl}$ and *Foxk2*$^{fl/fl}$ mice at 8 weeks old (*n=8*), including BV (b), BV/TV (c), TB.N (d) and TB.SP (e). (f and g) Quantitative analysis of biomechanics of the femurs from male and female *Osx-Cre;Foxk2*$^{fl/fl}$ and *Foxk2*$^{fl/fl}$ mice at 8 weeks old (Male: *n=7*; Female: *n=8*), including Max Bending Strength (f) and Elastic Modulus (g). (h) H&E staining of the femurs from male and female *Osx-Cre;Foxk2*$^{fl/fl}$ and *Foxk2*$^{fl/fl}$ mice at 8 weeks old. (i-k) Representative images (i) and quantitative analysis of calcein double labeling from male and female *Osx-Cre;Foxk2*$^{fl/fl}$ and *Foxk2*$^{fl/fl}$ mice at 8 weeks old (*n=3*), characterized as MAR (j) and BFR (k). (l) Representative images of OCN IHC staining in male and female *Osx-Cre;Foxk2*$^{fl/fl}$ and *Foxk2*$^{fl/fl}$ mice at 8 weeks old. (m) Quantification of OCN IHC staining *(n=5)*. (n) Representative images of Trap staining in male and female *Osx-Cre;Foxk2*$^{fl/fl}$ and *Foxk2*$^{fl/fl}$ mice at 8 weeks old. (o) Quantification of Trap staining (*n=5*). *$p < 0.05$, **$p < 0.01$, ***$p < 0.001$.

Figure 3

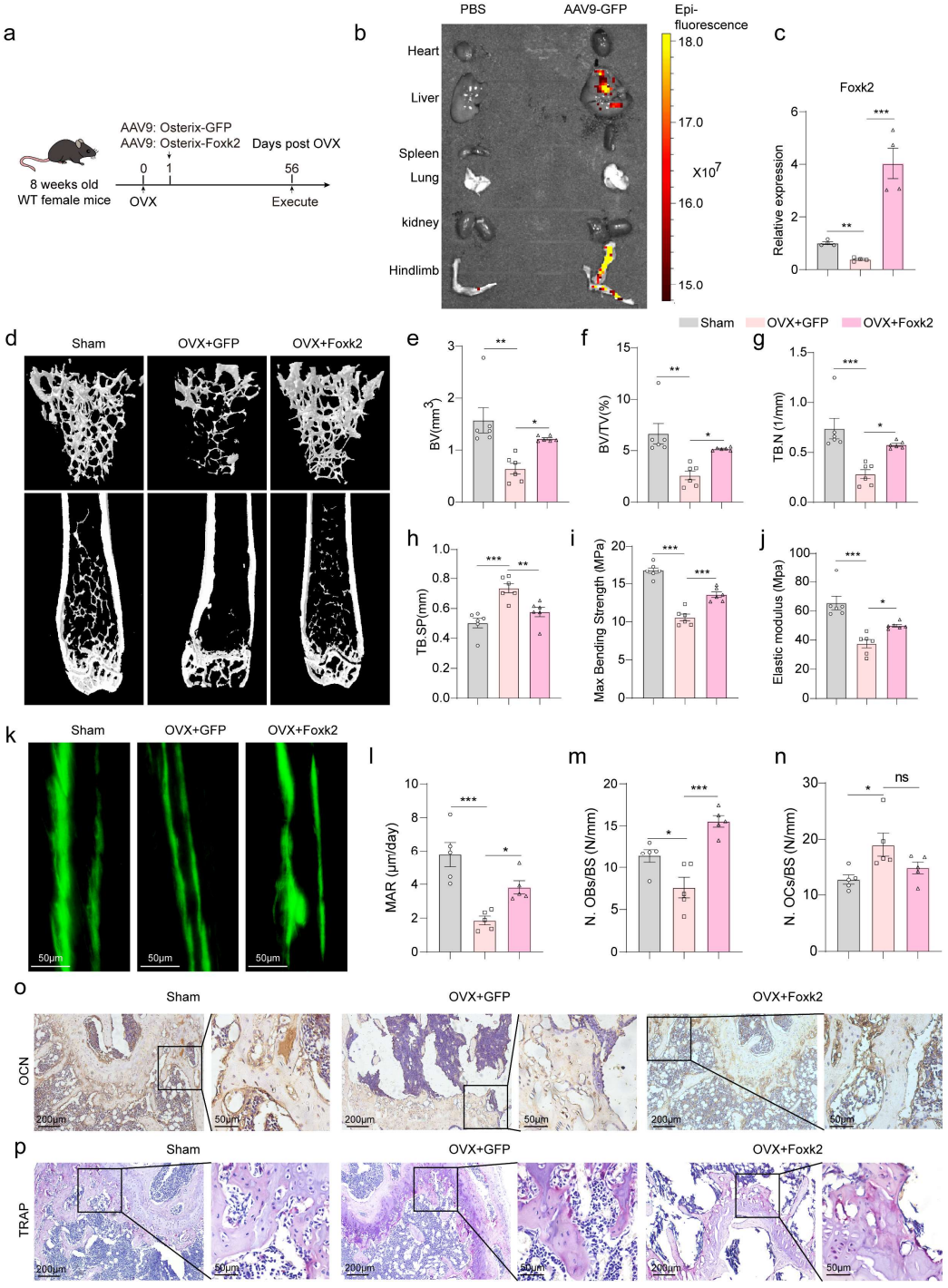


Figure 3. Overexpression of Foxk2 in pre-osteoblasts increases bone mass of osteoporotic mice. (a) Experimental design of OVX mice treated with AAV9-Osterix-Foxk2 via tail vein injection. Femurs from different groups were collected for further analysis at 56 days after surgery. (b) Representative images of the IVIS-100 optical imaging system used to monitor GFP expression in individual tissues. y-axis, radiant efficiency (p/s/cm2/ sr/μW/cm2). (c) qPCR was applied to quantify mRNA levels of

Foxk2 in femurs from treated sham and OVX mice (*n=4*). (d) Representative images of microCT analysis of treated sham and OVX mice including two-dimensional construction of distal femur and three-dimensional reconstruction of trabecular bone of distal femur. (e-h) Quantitative microCT analyses of the distal end of the femurs of treated sham and OVX mice (*n=6*), including BV (e), BV/TV (f), TB.N (g) and TB.SP (h). (i and j) Quantitative analysis of biomechanics of the femurs from treated sham and OVX mice (*n=6*), manifested as Max Bending Strength (i) and Elastic Modulus (j). (k and l) Representative images (k) and quantitative analysis (l) of calcein double labeling of treated sham and OVX mice (*n=5*), manifested as MAR. (m) Quantification of OCN IHC staining of treated sham and OVX mice *(n=5)*. (n) Quantification of Trap staining of treated sham and OVX mice *(n=5)*. (o) Representative images of OCN IHC staining of treated sham and OVX mice. (p) Representative images of Trap staining of treated sham and OVX mice. $*p < 0.05$, $**p < 0.01$, $***p < 0.001$.

Figure 4

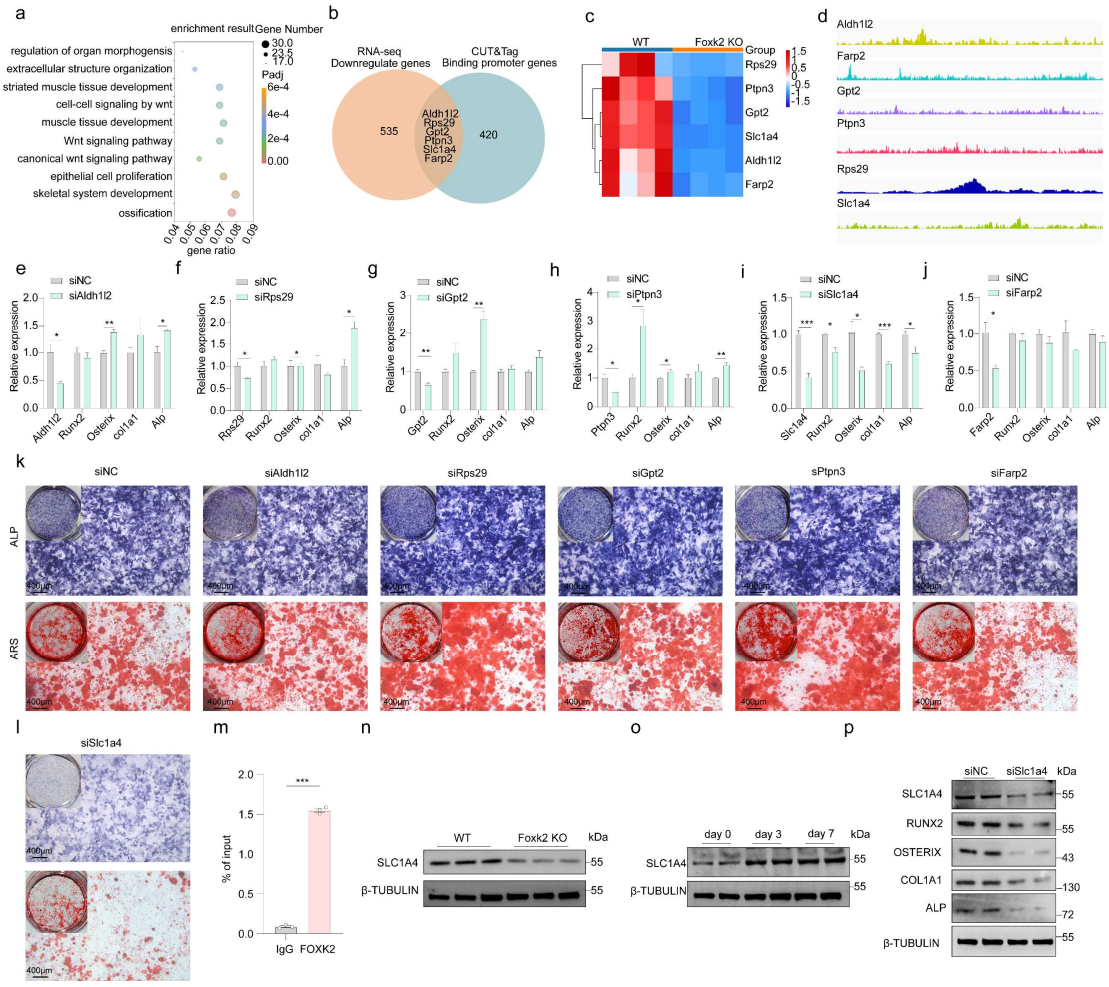


Figure 4. Slc1a4 has been identified as a direct target of Foxk2. (a) Gene Ontology (GO) analysis of downregulated genes in *Foxk2 KO* osteoblasts in RNA-seq data. (b) Overlaps between genes of downregulated by *Foxk2 KO* in RNA-seq data and promoter region is bound by FOXK2 in CUT&Tag data. (c) Heat map of candidate gene expression from data of RNA-seq. (d) IGV visual analyzed the FOXK2 biding regions of candidate genes. (e-j) qPCR was used to quantify corresponding candidate gene, Runx2, Osterix, Col1a1 and Alp mRNA levels after 7 days of siRNA (siAldh1l2 (e), siRps29 (f), siGpt2 (g), siPtpn3 (h), siSlc1a4 (i) and siFarp2 (j)) transfection in primary pre-osteoblasts ($n=3$). (k and l) Representative images of ALP and ARS staining of primary pre-osteoblasts after transfection with siRNA of each candidate gene. (m) Chromatin immunoprecipitation was performed in WT pre-osteoblasts with either IgG or FOXK2 and subsequently subjected to qPCR analysis with the indicated primers ($n=3$). (n) Western blot analysis of SLC1A4 protein levels in WT and *Foxk2 KO*

primary pre-osteoblasts. (o) Western blot analysis of SLC1A4 protein levels of primary pre-osteoblasts at days 0, 3, and 7 of osteogenic induction. (p) Western blot analysis of SLC1A4, RUNX2, OSTERIX, COL1A1 and ALP protein levels in siNC or siSlc1a4 transfected primary pre-osteoblasts. *$p < 0.05$, **$p < 0.01$, ***$p < 0.001$.

Figure 5

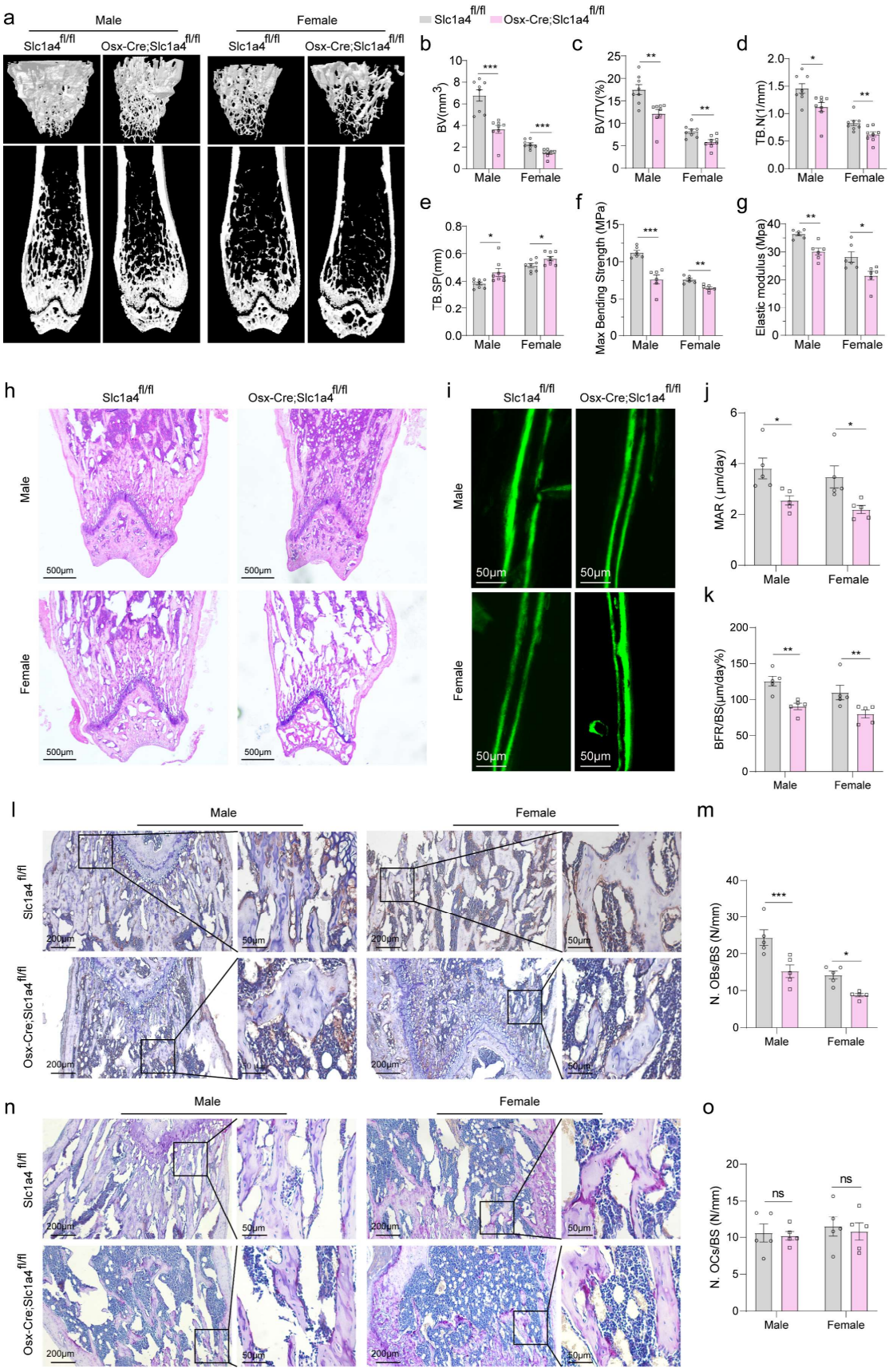


Figure 5. Deletion of Slc1a4 in Pre-osteoblasts impaired bone formation.

(a) Representative images of microCT analysis of male and female *Osx-Cre;Slc1a4$^{fl/fl}$* and Slc1a4$^{fl/fl}$ mice including two-dimensional construction of distal femur from 8-week-old male and female mice and three-dimensional reconstruction of trabecular bone of distal femur. (b-e) Quantitative microCT analyses of the distal end of the femurs from male and female *Osx-Cre;Slc1a4$^{fl/fl}$* and Slc1a4$^{fl/fl}$ mice at 8 weeks old (*n=8*), including BV (b), BV/TV (c), TB.N (d) and TB.SP (e). (f and g) Quantitative analysis of biomechanics of the femurs from male and female *Osx-Cre;Slc1a4$^{fl/fl}$* and Slc1a4$^{fl/fl}$ mice at 8 weeks old (*n=6*), including Max Bending Strength (f) and Elastic Modulus (g). (h) H&E staining of the femurs from male and female *Osx-Cre;Slc1a4$^{fl/fl}$* and Slc1a4$^{fl/fl}$ mice at 8 weeks old. (i-k) Representative images (i) and quantitative analysis of calcein double labeling from male and female *Osx-Cre;Slc1a4$^{fl/fl}$* and Slc1a4$^{fl/fl}$ mice at 8 weeks old (*n=5*), characterized as MAR (j) and BFR (k). (l) Representative images of OCN IHC staining in male and female *Osx-Cre;Slc1a4$^{fl/fl}$* and Slc1a4$^{fl/fl}$ mice at 8 weeks old. (m) Quantification of OCN IHC staining *(n=5)*. (n) Representative images of Trap staining in male and female *Osx-Cre;Slc1a4$^{fl/fl}$* and Slc1a4$^{fl/fl}$ mice at 8 weeks old. (o) Quantification of Trap staining (*n=5*). *$p < 0.05$, **$p < 0.01$, ***$p < 0.001$.

Figure 6

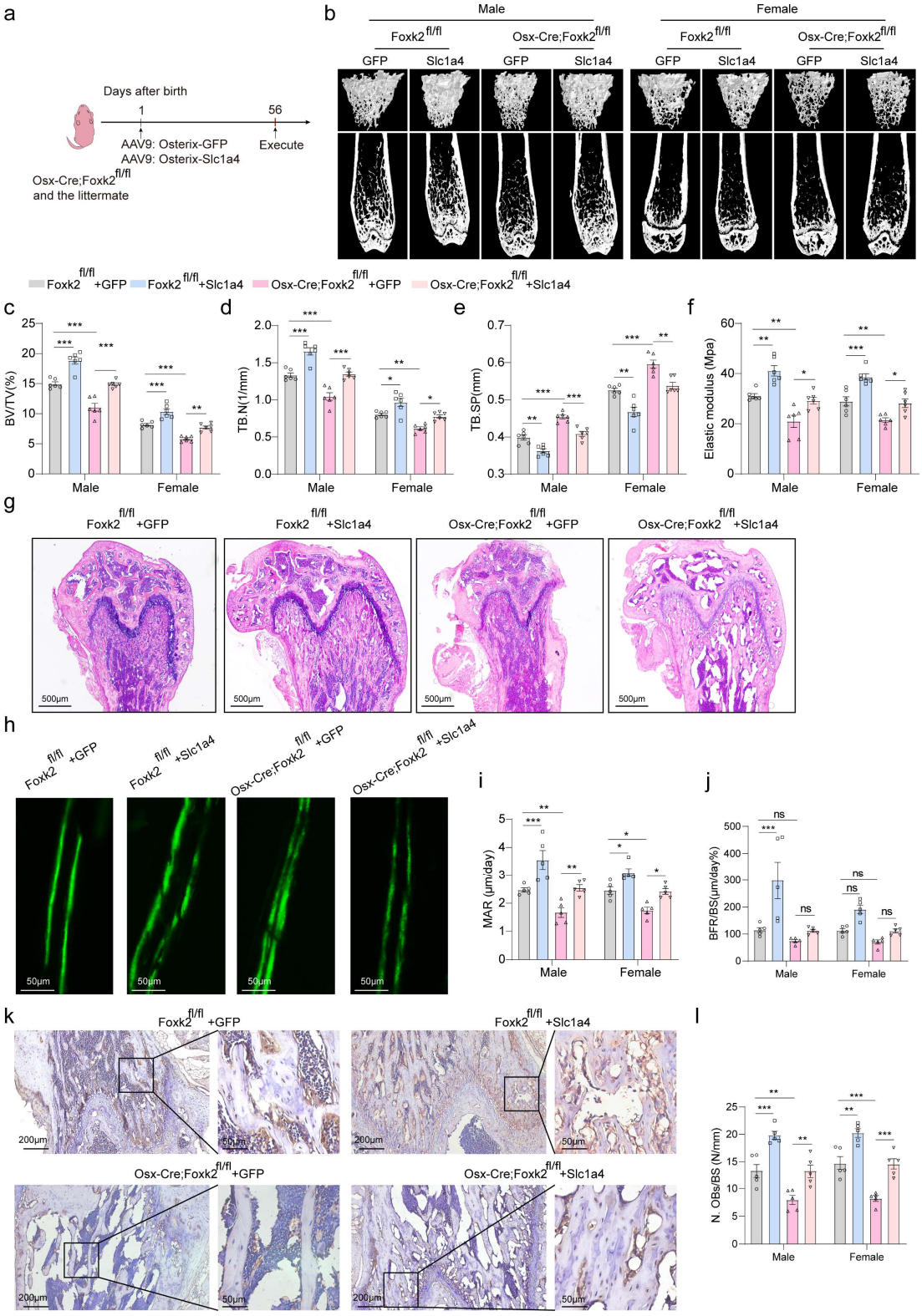


Figure 6. Slc1a4 functions as a direct downstream mediator of Foxk2 in bone formation. (a) Experimental design of *Foxk2*$^{fl/fl}$ and *Osx-Cre;Foxk2*$^{fl/fl}$ mice treated with AAV9-Osterix-GFP or AAV9-Osterix-Slc1a4 via tail vein injection. Femurs from

different groups were collected for further analysis after 56 days of birth. (b) Representative images of microCT analysis of treated male and female *Foxk2*$^{fl/fl}$ and *Osx-Cre;Foxk2*$^{fl/fl}$ mice including two-dimensional construction of distal femur and three-dimensional reconstruction of trabecular bone of distal femur. (c-e) Quantitative microCT analyses of the distal end of the femurs of treated male and female *Foxk2*$^{fl/fl}$ and *Osx-Cre;Foxk2*$^{fl/fl}$ mice ($n=6$), including BV/TV (c), TB.N (d) and TB.SP (e). (f) Quantitative analysis of biomechanics of the femurs from treated male and female *Foxk2*$^{fl/fl}$ and *Osx-Cre;Foxk2*$^{fl/fl}$ mice ($n=6$), characterized as elastic modulus. (g) Representative images of H&E staining of treated male *Foxk2*$^{fl/fl}$ and *Osx-Cre;Foxk2*$^{fl/fl}$ mice. (h) Representative images of calcein double labeling of treated male *Foxk2*$^{fl/fl}$ and *Osx-Cre;Foxk2*$^{fl/fl}$ mice. (i, j) Quantitative analysis of calcein double labeling of treated male and female *Foxk2*$^{fl/fl}$ and *Osx-Cre;Foxk2*$^{fl/fl}$ mice ($n=5$), quantified as MAR (i) and BFR (j). (k) Representative images of OCN IHC staining of treated male *Foxk2*$^{fl/fl}$ and *Osx-Cre;Foxk2*$^{fl/fl}$ mice. (l) Quantification of OCN IHC staining of treated male and female *Foxk2*$^{fl/fl}$ and *Osx-Cre;Foxk2*$^{fl/fl}$ mice ($n=5$). $*p < 0.05$, $**p < 0.01$, $***p < 0.001$.

Figure 7

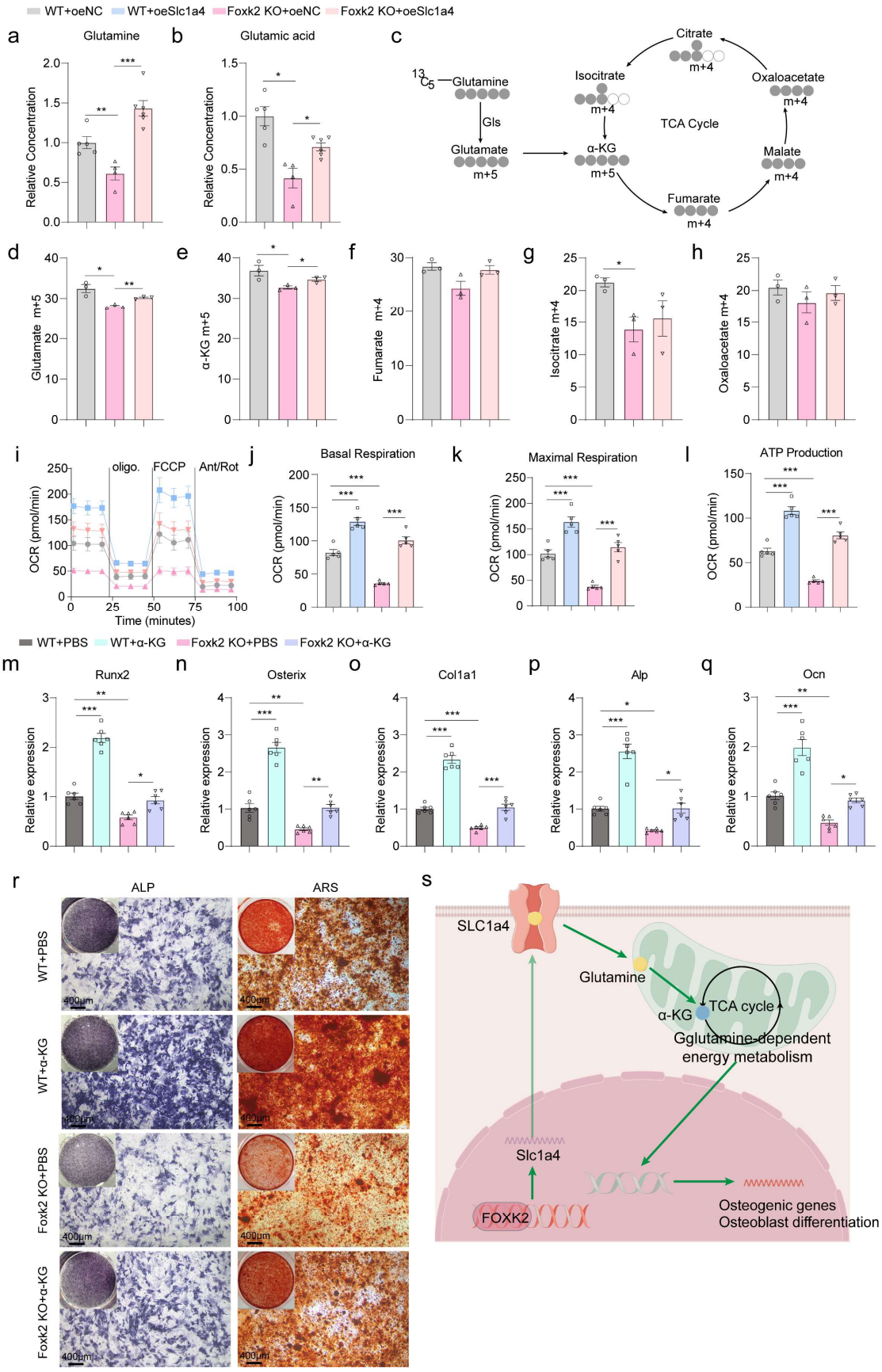


Figure 7. Foxk2/Slc1a4 promotes glutamine-dependent energy metabolism of

osteoblasts. (a and b) Effect of Foxk2/Slc1a4 axis on intracellular glutamine (a) and glutamic acid (b) concentration measured by mass spectrometry in WT and *Foxk2 KO* primary pre-osteoblasts treated with control plasmids (oeNC) or Slc1a4 overexpression plasmids (oeSlc1a4) (WT+oeNC: *n=5*, Foxk2 KO+oeNC: *n=4*, Foxk2 KO+oeSlc1a4: *n=6*). (c) Schematic representation of $^{13}C_5$-glutamine tracing. Filled circles indicate ^{13}C, and open circles denote ^{12}C. α-KG is α-ketoglutarate. (d-h) Isotopic labeling of glutamate (d), α-KG (e), Fumarate (f), Isocitrate (g), and oxaloacetate (h) (*n=3*). (i-l) The oxygen consumption rate in WT and *Foxk2 KO* primary pre-osteoblasts treated with control plasmids or Slc1a4 overexpression plasmids was measured using Seahorse XF assay. Basal respiration (j), Maximal respiration (k) and ATP production (l) were analyzed (*n=5*). (m-q) qPCR quantified mRNA levels of Runx2 (m), Osterix (n), Col1a1 (o), Alp (p), and Ocn (q) in WT and *Foxk2 KO* primary pre-osteoblasts treated with PBS or α-KG (*n=6*). (r) The representative ALP and ARS staining of WT and *Foxk2 KO* primary pre-osteoblasts treated with PBS or α-KG. (s) Proposed working model of Foxk2 in regulating osteoblast differentiation through Slc1a4-regulated glutamine-dependent energy metabolism. *$p < 0.05$, **$p < 0.01$, ***$p < 0.001$.

Supplementary Files

This is a list of supplementary files associated with this preprint. Click to download.

- Supplementarymaterials.pdf